ELSEVIER

Journal of Molecular Catalysis A: Chemical 131 (1998) 185–197

JOURNAL OF MOLECULAR CATALYSIS A: CHEMICAL

A combined STM/molecular beam study of formic acid oxidation on Cu(110)

Michael Bowker [a,*], Stephen Poulston [a,b], Roger A. Bennett [a,b], Peter Stone [a], Adrian H. Jones [c], Sam Haq [b], Peter Hollins [a]

[a] *Catalysis Research Centre, University of Reading, Department of Chemistry, Whiteknights, Reading, RG6 6AD, UK*
[b] *Interdisciplinary Research Centre in Surface Science, University of Liverpool, Liverpool, L69 3BX, UK*
[c] *Oxford Instruments, Chesterton Mills, French's Road, Cambridge, CB4 3NP, UK*

Received 25 June 1997; accepted 6 August 1997

Abstract

In this paper, we describe a powerful combination of methods used to elucidate the mechanisms and kinetics of surface reactions, namely, molecular beam reactor work and scanning tunnelling microscopy (STM). These two combine microkinetic measurements with a technique which has atomic spatial resolution for structural determination during the course of a reaction. This gives the ability to link the worlds of macroscale and nanoscale surface chemistry. A particular application is highlighted here, namely, the adsorption and oxidation of formic acid on Cu(110), in principle, a simple reaction, which turns out to be very complicated. The findings can be summarised as follows: (i) predosed oxygen enhances formic acid sticking by at least an order of magnitude; (ii) oxygen predosed to a coverage below 0.25 monolayers is completely removed as water by the reaction with formic acid to produce formate; (iii) above this oxygen coverage, some oxygen remains on the surface after reaction and is compressed up into the locally higher coverage $c(6\times2)$ structure, otherwise only obtained by extremely high exposures of oxygen; (iv) the reaction stoichiometry changes from 2 HCOOH: 1 $O_{(a)}$ to 1:1 at high temperature where the formate is unstable; (v) gross rearrangement and redistribution of Cu atoms occurs during the course of the reaction; and (vi) the formate adsorbate structure varies considerably with substrate temperature, oxygen precoverage and formic acid exposure, five distinct structures being observed with STM. © 1998 Elsevier Science B.V.

Keywords: Scanning tunnelling microscopy (STM); Molecular beam; Formic acid; Oxidation; Copper

1. Introduction

In principle, it is straightforward to analyse a simple heterogeneously catalysed reaction of the following kind:

$$A + B \rightarrow C + D + \ldots$$

for which the Langmuir–Hinshelwood kinetics apply, that is,

$$\text{Rate} = k\left[A_{(a)}\right]\left[B_{(a)}\right]$$

where the subscripts indicate adsorbed reactants.

However, the problem is that there are at least five different rate constants involved (surface reaction and adsorption and desorption

* Corresponding author.

PII S1381-1169(97)00265-3

for reactants) and these constants are often very strong functions of the coverage of both reactants. Furthermore, these coverage functions are complicated, determined by lateral interactions between species in the surface, by diffusion in the weakly held molecular states, and by surface atom rearrangements such as reconstructions which may occur as the coverage alters with changing conditions.

These considerations are of great importance to catalysis which is advancing to the stage where new catalysts will be designed by computer-based expert systems. These will include kinetic prediction routines such as the microkinetic analysis method described by Dumesic et al. [1] which can direct catalyst synthesis efforts to focus on the rate-determining step under any particular set of conditions. Thus, understanding the details of the kinetics for particular reactions is crucial. It is essential to achieve an understanding of such phenomena on both single crystals and catalysts. However, it is often difficult to obtain detailed, non-averaged kinetic information from the latter, hence, the advantage of using the former type of substrate.

In this paper, we describe the application of kinetic, dynamic and structural analysis methods to the study of a catalytically relevant surface reaction. The kinetics are probed by a molecular beam reactor and the structural and dynamic aspects by scanning tunnelling microscopy (STM). The particular advantage of this combination is that the molecular beam gives us macroscale kinetic information while STM gives us the ability to link this data to events on the nanoscale at atomic resolution and often in real time.

2. Experimental

2.1. The STM

STM experiments were performed using an Oxford Instruments variable temperature STM partly based on the design of the FOM Institute, which has been described in detail elsewhere [2]. The STM was contained within a UHV chamber equipped with additional facilities for Ar^+ ion sputtering, low energy electron diffraction (LEED) and Auger electron spectroscopy (AES). Both LEED and AES measurements were carried out using a three-grid retarding field analyser with integral electron gun. Temperature programmed desorption (TPD) and residual gas analysis were performed using a quadrupole mass spectrometer. The chamber was ion pumped to produce a typical base pressure of 1×10^{-10} mbar while additional pumping for high gas loads, during sputtering and the initial stages of bakeout, was available from a turbomolecular pump backed by a rotary pump. Gas dosing was carried out by backfilling the chamber. Using a wobble stick, the sample holder with integral heater and thermocouple could be transferred within the chamber between the STM stage and a manipulator which allowed access to the other experimental techniques. A schematic of the chamber layout is shown in Fig. 1a. The sample was heated both radiatively and if necessary, with electron bombardment using a tungsten filament situated close to the back face of the crystal. During scanning, the sample was placed horizontally with the scanner above offset to one edge to allow coarse approach of the sample to the tip via a sample tilting mechanism, as shown in Fig. 1b. Overlayer coverages are quoted in monolayers (ML) where 1 ML is the number density of atoms in the surface layer of Cu(110). Gas exposures are quoted in Langmuirs (L) where $1\ \mathrm{L} = 1 \times 10^{-6}$ Torr s.

The Cu(110) sample was cleaned using cycles of Ar^+ ion bombardment (500 eV, 10 μA) at 720 K, cooling to room temperature in the ion beam and vacuum annealing to 720 K. This procedure produced a good (1×1) LEED pattern and left no detectable trace of sulphur or carbon in AES.

The images reported here are raw data, except for a simple global plane subtraction. They are not filtered or manipulated in any other way.

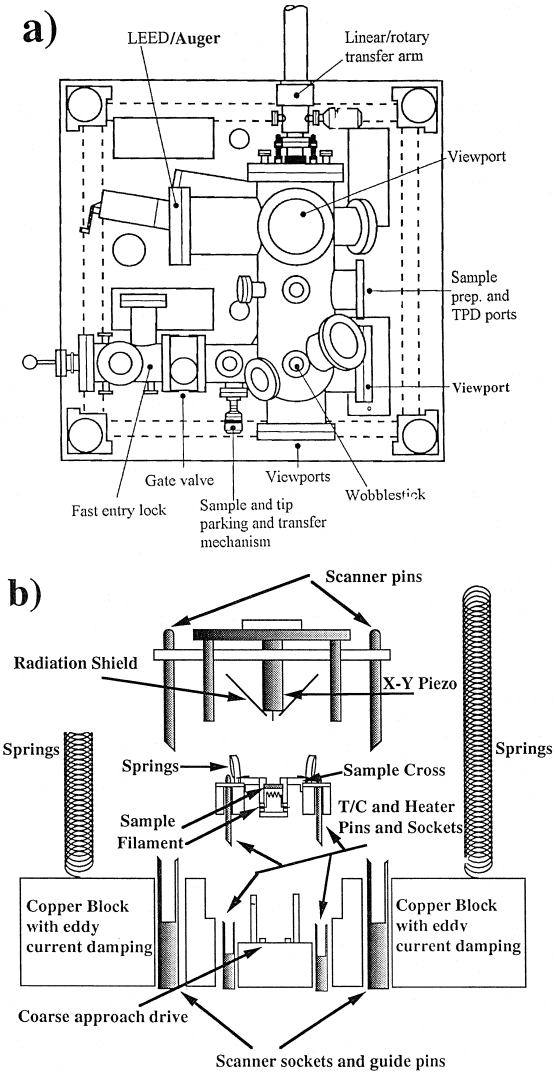

Fig. 1. (a) Schematic of the STM used in this work. (b) Close up schematic of the sample/scanner assembly.

Bias voltages quoted in the figure captions are sample biases relative to the tip.

2.2. The molecular beam reactor

The aim of the molecular beam system, which has been described in detail elsewhere [3], is to produce a collimated beam of thermal gas molecules that can be directed at a crystal surface. For the types of experiment described in this publication, it is essential to obtain a reasonable beam intensity from low vapour pressure materials, preferably with only a few mbar pressure in the gas line. The beam originates in an heatable source capillary made of quartz with an internal diameter of 0.2 mm. The beam is formed through a conical skimmer and final defining collimator and the whole is designed to produce a constant flux across the beam diameter at the sample, with a minimised penumbra of varying intensity. This is absolutely necessary for obtaining the correct dependence of sticking probability (S) upon coverage. The in-beam pressure of gas molecules is approximately 1×10^{-7} mbar.

The reactor can be run in several modes.

(i) Transient mode: here, one reactant is dosed first and then the other reactant is introduced in a sequential manner.

(ii) Steady state mode: here, both reactants are in the beam simultaneously and are directed at the crystal which is held at fixed temperature.

(iii) Temperature programmed mode: this uses either mixed beam or single species dosing while slowly ramping the crystal temperature to measure the temperature dependence of reaction probability, uptake and product evolution.

(iv) Pseudo-steady state mode: step jumps in temperature are employed to carry out near isothermal rate measurements relatively quickly for mixed or single species beams.

These modes have been described in more detail in an earlier review [4]. In this paper, we will describe the application of STM and molecular beam techniques to a particular system, the reaction of formic acid with Cu(110), and this uses only mode (i) above.

3. Application to a real system

The reaction of formic acid with surfaces is of great relevance to catalysis as evidenced by an early review article on that subject by Mars et al. [5]. It is so important because it represents a simple organic molecule which can react in

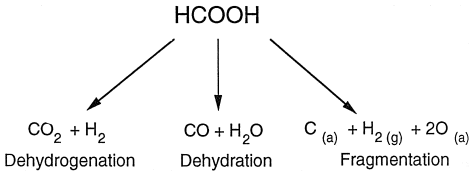

Fig. 2. Outline of the decomposition pathways of formic acid.

several ways, as shown in Fig. 2; first, by complete fragmentation, secondly, by dehydrogenation, thirdly, by dehydration. Further, it is implicated as a direct intermediate in several large scale catalytic reactions including, as shown in Fig. 3, methanol synthesis [6] and oxidation which involve a common pathway. The formate has been proposed to be the most stable and abundant surface intermediate in methanol synthesis, while it is the non-selective intermediate involved in the oxidative dehydrogenation of methanol. Thus, an understanding of its stability and structure on surfaces is of significance to the catalytic community.

4. Results and discussion

4.1. Molecular beam studies of formic acid oxidation

The interaction of formic acid with Cu(110) has been studied using the molecular beam system described above, with the results shown in Figs. 4 and 5. Fig. 4 shows the variation of S with formic acid uptake at room temperature where the formate intermediate is produced without decomposition. The initial reactive sticking coefficient (S_0) at room temperature is low on the clean surface at ~ 0.1 (Fig. 5) but is enhanced significantly on the oxygen predosed surface to 0.8 (Fig. 4), even with small amounts of oxygen predosed. In the case of oxygen precovered surfaces, formic acid uptake is accompanied by water desorption. From these data, we can deduce several things.

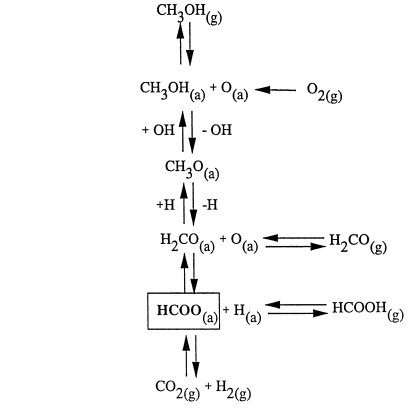

Fig. 3. The position of formate as a key intermediate in the reaction pathway of methanol synthesis and methanol oxidation.

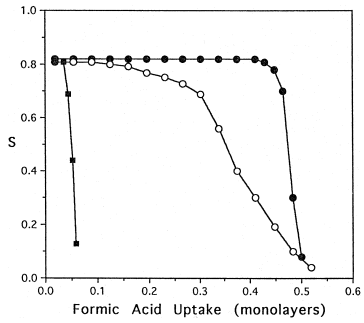

Fig. 4. Molecular beam data showing the variation in sticking probability, S, with formic acid uptake for the adsorption of formic acid at room temperature on oxygen precovered Cu(110). Open circles, 0.5 ML oxygen precoverage; filled circles, 0.25 ML oxygen; filled squares, 0.03 ML oxygen.

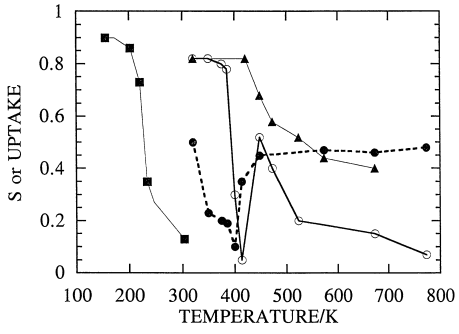

Fig. 5. Variation of the initial sticking probability and uptake (at the point where S falls below 0.05) as a function of substrate temperature for formic acid adsorption on clean and oxygen predosed Cu(110). Sticking: filled squares, clean surface; filled triangles, 0.25 ML oxygen precoverage; open circles, 0.5 ML oxygen precoverage. Filled circles, formic acid uptake in monolayers.

(i) The oxygen sites act as high activity centres for formic acid reactions, greatly enhancing sticking probability.

(ii) Formic acid adsorbs reversibly into a weakly held state which can diffuse widely (in atomic terms) over the surface during its short sojourn there, and can thus, 'find' oxygen atoms with high probability even though they may be few in number at the surface [7]. This is demonstrated by the high initial sticking probability (S_0) on the surface predosed with only 0.03 ML oxygen and, with higher oxygen precoverages, by the flat profile of S vs. uptake up until most of the oxygen has been used up (Fig. 4).

(iii) For initial oxygen coverages of up to 0.25 ML, the formic acid titrates off the oxygen by the following overall reaction scheme, producing twice as much formate adsorbed as predosed oxygen atoms removed leading to a total uptake of 0.5 ML formate when all the oxygen has reacted

$$2HCOOH_{(g)} + O_{(a)} \rightarrow H_2O_{(g)} + 2HCOO_{(a)}.$$

(iv) Above a predose of 0.25 ML of oxygen, the amount of formate produced remains approximately the same, at 0.5 ML. This is a consequence of some oxygen atoms remaining co-adsorbed on the surface which are much less reactive, as described in more detail in Section 4.2 below.

Evidence that formate is produced on the Cu(110) surface by such dosing has been confirmed by a range of surface spectroscopies, including UPS, XPS [8] RAIRS [9,10] SEXAFS and NEXAFS [11]. The O(1s) XPS shows a single peak, indicating that the two formate oxygen atoms are equivalent, while the RAIRS is dominated by the symmetric COO stretching vibration at 1355 cm^{-1} characteristic of bidentate formate. Photoelectron diffraction and SEXAFS show the molecule to be upright on the surface bonded in an aligned bridge site [12].

Pioneering experiments by Falconer and Madix [13], Ying and Madix [14], and Madix and Telford [15] first showed something of the kinetics and mechanism of formate decomposition using TPD. These revealed a formate decomposition rate limited peak with coincident evolution of CO_2 and H_2 at 450 K, showing the high stability of the formate on Cu(110), reflecting the low reactivity of this metal. Only the dehydrogenation pathway was observed. Other metals decompose formate at much lower temperatures, for instance, below 300 K on Ni(110) [16] and 140–237 K on Pd(110) [17], both showing some evidence of dehydration.

However, that early work did not reveal the complexity of the dependence of the reaction on oxygen coverage and temperature. The ability to study such effects is aided by the molecular beam measurement, which can be carried out isothermally and at temperatures well above the desorption peak temperature.

With increasing reaction temperature, the reaction stoichiometry changes from 2:1 to 1:1 due to the following reaction:

$$HCOOH_{(g)} + O_{(a)} \rightarrow CO_{2(g)} + H_2O_{(g)}.$$

This is due to the interplay between the following steps:

$$HCOOH_{(g)} \rightarrow HCOOH_{(a)},$$

$$HCOOH_{(a)} + O_{(a)} \rightarrow HCOO_{(a)} + OH_{(a)},$$

$$HCOOH_{(a)} + OH(a) \rightarrow HCOO(a) + H_2O_{(g)},$$

$$H_{(a)} + OH_{(a)} \rightarrow H_2O_{(g)},$$

$$HCOO_{(a)} \rightarrow H_{(a)} + CO_{2(g)},$$

$$2H_{(a)} \rightarrow H_{2(g)}.$$

The interaction of the first acid molecule with an oxygen atom gives a hydroxyl group which can then further react (i) with another formic acid to produce water and another formate, or (ii) with a hydrogen atom to produce a water molecule directly. (ii) is only favoured when the decomposition rate of the acid be-

comes significant (at high temperature) to produce available hydrogen atoms. Thus, the reaction stoichiometry, in terms of formate/oxygen ratio, starts to decrease near the beginning of the formate decomposition curve shown by the TPD [13–15,18].

The initial reaction probability diminishes at higher temperature, Fig. 5, probably due to the reduced diffusion length of the weakly held precursor molecule [7]. However, the reaction probability increases during the course of the reaction for reasons outlined below.

Very unusual behaviour is measured for a surface predosed with 0.5 ML of oxygen as shown in Fig. 5. At 300 K the behaviour is similar to the 0.25 ML oxygen case (Fig. 4), but the sticking probability decreases more rapidly as the oxygen is reacted (i.e., at higher formic acid uptake). Furthermore, the initial sticking probability, S_0, dependence on substrate temperature, Fig. 5, is complicated showing a sharp drop at 380 K which is recovering by 480 K. In addition, the formic acid uptake (at the point where S falls to around 0.05) decreases to $\sim$ 0.18 ML by 403 K, and then increases again at higher temperature. This strong reduction in the uptake is mainly a consequence of changes in the adsorbate structure, as the following STM results help clarify.

4.2. STM results

In order to interpret the STM data, it is informative to review the known structures of oxygen on Cu(110). Oxygen adsorption at room temperature generates a (2×1) added row structure in which oxygen molecules dissociatively adsorb, diffuse and capture Cu adatoms which are thermally generated by evaporation from the Cu surface step edges (a solid/vapour equilibrium in two dimensions). These units form long chains of alternating O–Cu atoms which lie along the [001] direction with attractive lateral forces between chains. Thus, at low coverages long thin islands of O-(2×1) form on the clean surface, while at higher coverages

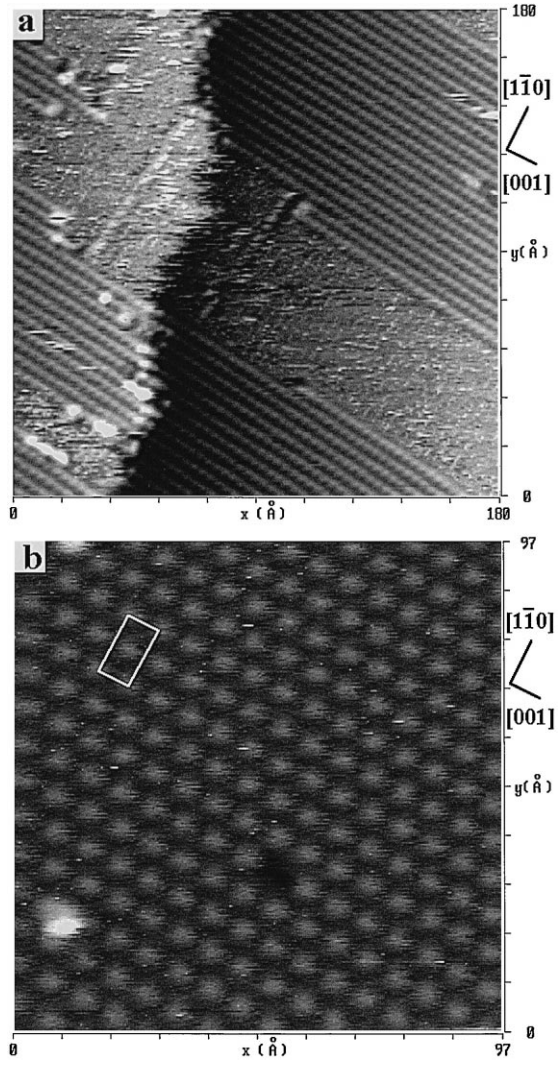

Fig. 6. STM images of oxygen structures on Cu(110). (a) Partial coverage ($\sim$0.3 ML) of O-(2×1), 180×180 Å, 1 nA, 100 mV. The origin of the bright streak along [1$\bar{1}$0] direction between the oxygen islands just to the left of the step edge is unclear but maybe an adatom rapidly diffusing along the copper rows (b) $c(6\times2)$ with unit cell outlined, 97×97 Å, 1 nA, -500 mV.

the chains merge to form wider islands, Fig. 6a. At elevated temperature (575 K) and very high oxygen exposures (20 000 L), a higher coverage $c(6\times2)$ structure forms, Fig. 6b, consisting of 2/3 ML oxygen and 5/6 ML added copper [19] which may be considered to be a precursor to oxidation of the copper. These surface structures have been well characterised and are shown schematically in Fig. 7. The super Cu atoms

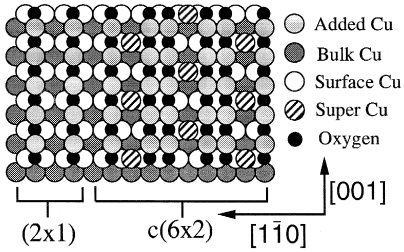

Fig. 7. Schematic showing the surface structure of the oxygen (2×1) and $c(6\times2)$ overlayers.

shown in the schematic of the $c(6\times2)$ structure are the most prominent feature of this structure observed in the STM image shown in Fig. 6b.

Exposure of the clean Cu(110) surface to ~10 L formic acid at 300 K resulted in observation of an overlayer structure using STM [20] (Fig. 8) which consisted of domains containing short rows parallel to the direction, with an inter-row spacing in the [001] direction of 2 lattice spacings of the unreconstructed 1×1-Cu(110) termination. Adjacent domains were offset in the [001] direction by 1 lattice spacing giving relatively short range order in [1$\bar{1}$0] direction. No ordered overlayer pattern was observed using LEED. The STM data and the

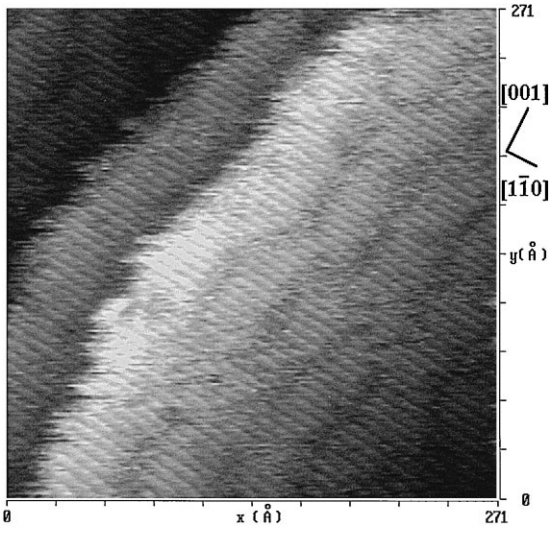

Fig. 8. STM image of formate on Cu(110) following exposure of the clean surface to ~10 L formic acid at 300 K, 271×271 Å, 1 nA, 498 mV.

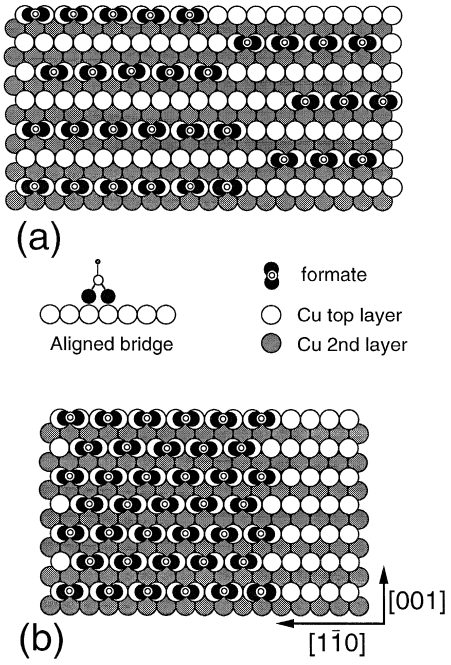

Fig. 9. Proposed structural model for (a) STM image in Fig. 8, (b) $c(2\times2)$ formate overlayer.

proposed structure, shown in Fig. 9a, are in good agreement with conclusions drawn with the use of other techniques including RAIRS [9] and PhD [12], in particular, the adsorption geometry, which is aligned bridge as indicated at the bottom of Fig. 9a, and the coverage; estimated at 0.25 ML from RAIRS data [9] and ~0.3 ML from our molecular beam data.

Fig. 10 shows a sequence of STM images taken at 300 K for a surface precovered with ~0.2 ML oxygen and then exposed to formic acid. We have been able to follow the reaction with STM while dosing formic acid allowing us to identify complex transformations of the overlayer structure and revealing the transient presence of a number of formate-related structures. Initially, adsorption and reaction resulted in replacement of the O-(2×1) structure with (3×1) and (4×1) structures which we assign to adsorbed formate, all these structures are shown in Fig. 10a. Both the (3×1) and (4×1) structures contain rows running parallel to the [001], the separation along the [1$\bar{1}$0] direction between

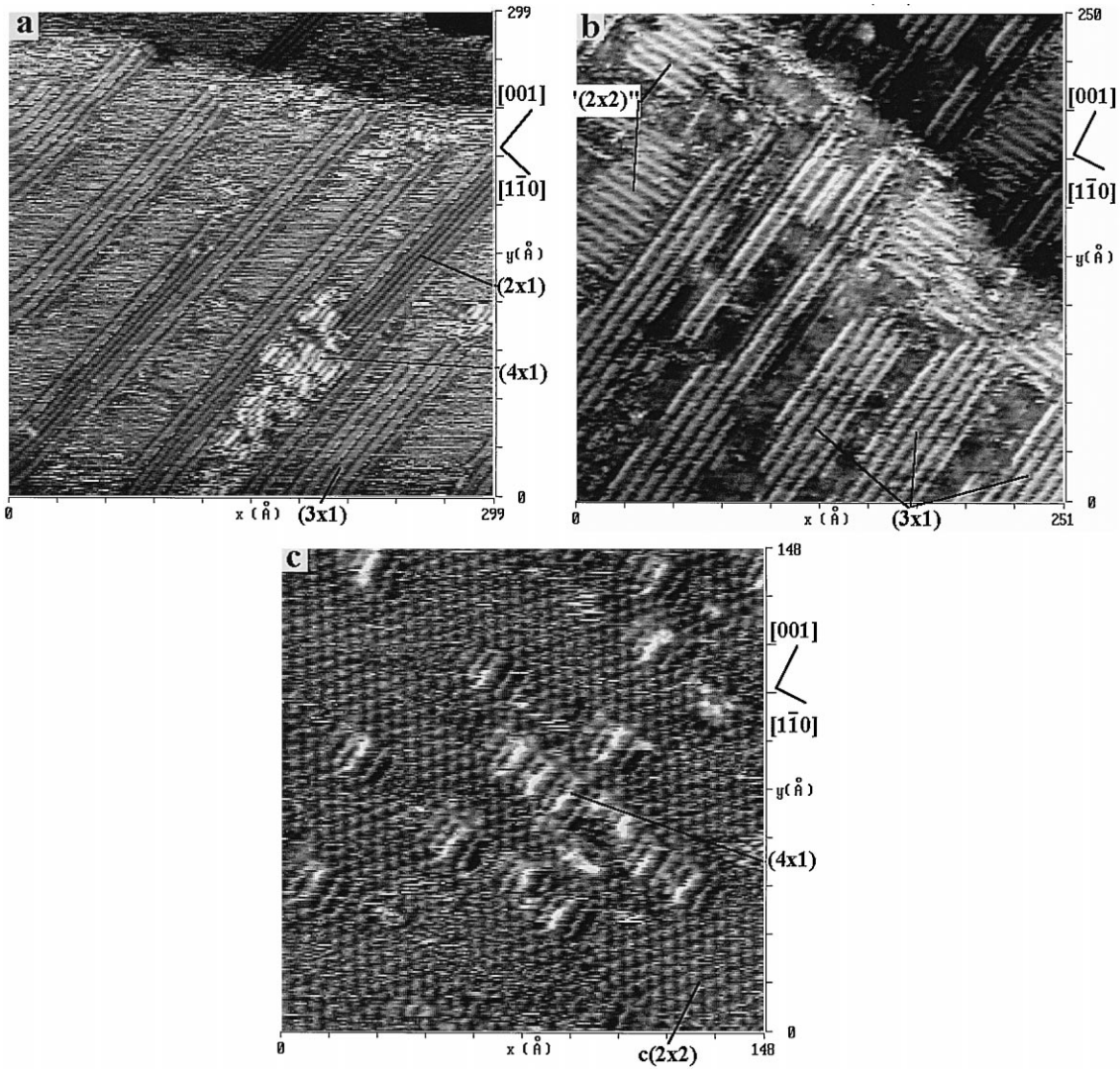

Fig. 10. STM images following the development of the adsorbate structures when Cu(110) precovered with ~0.2 ML oxygen was exposed to formic acid at 300 K. (a) Long thin islands of mostly formate (3×1) together with a small amount of O-(2×1) and formate (4×1), 299×299 Å, 1 nA, −500 mV. (b) Formate (3×1) together with the '2×2' formate structure observed on the clean surface (see Fig. 8 and associated text), 251×251 Å, 1 nA, −500 mV. (c) Formate $c(2\times2)$ together with small areas of formate (4×1), 148×148 Å, 1 nA, −500 mV.

equivalent parts of the structure being three and four lattice spacings, respectively. Both structures are described in more detail below. This was followed, with continued formic acid exposure, by the additional appearance of the formate structure produced by formic acid adsorption on clean Cu in the regions of the surface which were initially free of oxygen, Fig. 10b. Continued dosing eventually resulted in the production of a formate $c(2\times2)$ overlayer structure as previously reported [21], this process being accompanied by the complete removal of the initial O-(2×1) structure. Fig. 10c was taken shortly before completion of the $c(2\times2)$ overlayer and shows mostly this structure, however, there are also small regions of the (4×1) formate structure. The final $c(2\times2)$ structure was also seen using LEED and the proposed

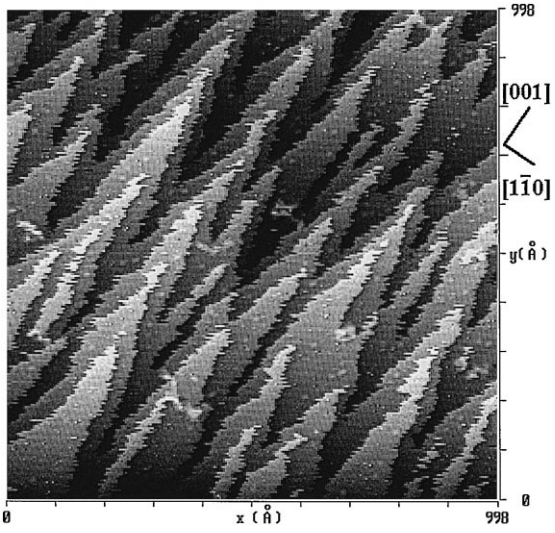

Fig. 11. STM image showing the sawtooth reconstruction effect produced by formic acid adsorption at 300 K on Cu(110) precovered with ~0.25 ML oxygen, 998×998 Å, 1 nA, −500 mV. The surface is completely covered in the $c(2\times2)$ formate structure.

structure is shown in Fig. 9b. The exact sequence and relative amounts of the different structures produced by formic acid adsorption on subsaturation oxygen coverages varies with the oxygen precoverage; the example presented here is, however, a good example of the complexity of the reaction. Formation of the $c(2\times2)$ structure is accompanied by the appearance of a sawtooth reconstruction of the step edges which in some cases can be quite extensive, as seen from the example in Fig. 11.

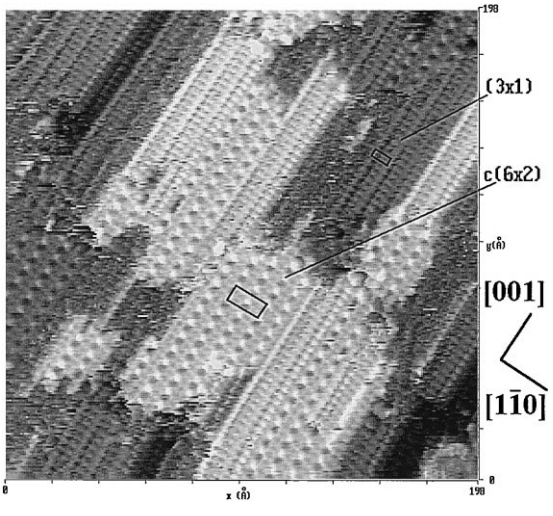

Fig. 12. STM image of the (3×1) formate and oxygen $c(6\times2)$ phases produced by formic acid adsorption at 300 K on Cu(110) precovered with 0.5 ML oxygen. Unit cells marked on the image.

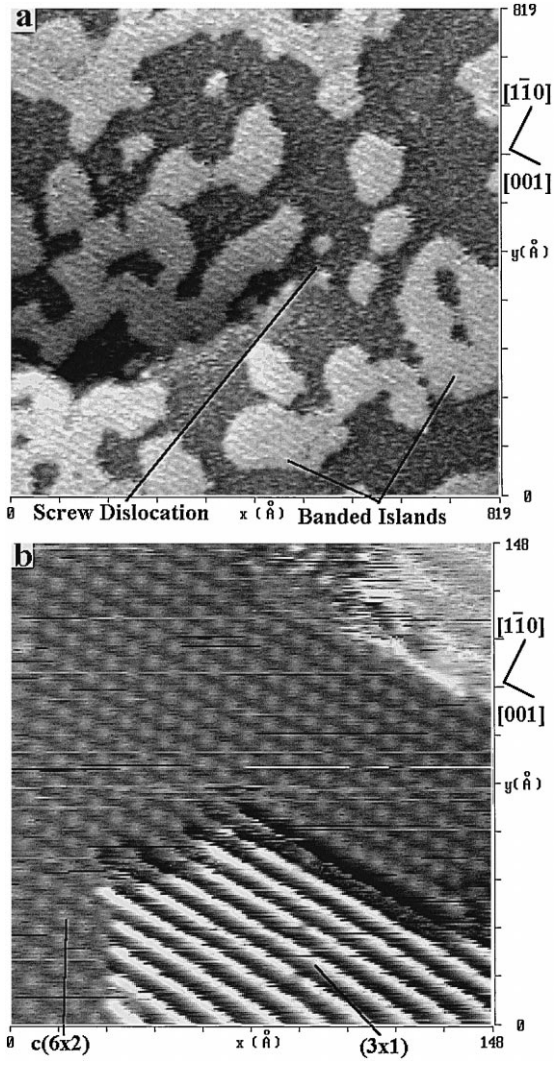

Fig. 13. STM images showing the different adsorbate phases produced by formic acid adsorption on a complete O-$c(6\times2)$ overlayer at 300 K. (a) Showing banded islands after 100 L exposure, 819×819 Å, 1 nA, −500 mV, a screw dislocation is marked on the image. (b) Showing an earlier stage of the reaction (250 L) where some $c(6\times2)$ remain together with formate (3×1) and a small region of the banded island structure in the top right hand corner of the image, 148×148 Å, 1 nA, −500 mV.

Formic acid exposure at 300 K on a surface precovered with 0.5 ML oxygen resulted in formation of separate phases of formate (3×1) and oxygen $c(6 \times 2)$ [18,22] Fig. 12. The appearance of the (3×1) formate structure varies considerably with sample bias, but at certain imaging conditions, it is clear that the unit cell contains two non-equivalent units, as is the case in Fig. 12. The implication this raises for the structure of the (3×1) phase is discussed below. The oxygen in the $c(6 \times 2)$ phase was significantly less reactive than that in the (2×1) phase but with continued dosing further reaction did occur leading to the gradual loss of these well ordered structures and the formation of small islands containing faint bands running parallel to the [001] direction with the remainder of the surface consisting of a disordered phase [22]. A very similar overlayer was observed using STM when a complete overlayer of $c(6 \times 2)$ was exposed to formic acid at 300 K [23], Fig. 13a, and was again preceded by the formation of coexisting regions of (3×1) and $c(6 \times 2)$, Fig. 13b. LEED and STM observations for the exposure of the complete $c(6 \times 2)$ overlayer to formic acid confirm the low reactivity of this surface, with the exposures required for reaction being two orders of magnitude greater than those for the (2×1) oxygen structure.

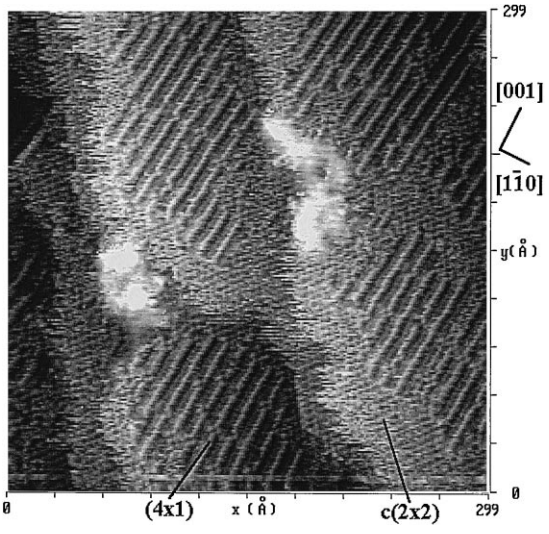

Fig. 14. STM image of the formate (4×1) structure formed by exposing a complete overlayer of O-(2×1) to 50 L formic acid at 300 K then annealing to 380 K, 299×299 Å, 1 nA, −500 mV.

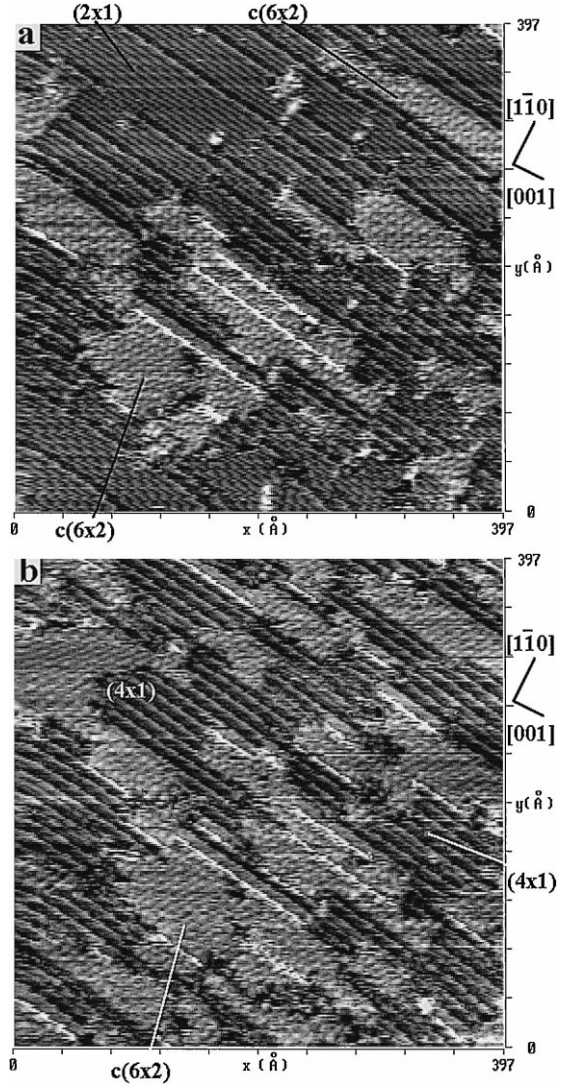

Fig. 15. STM images following the reaction of a complete O-(2×1) overlayer with formic acid at 350 K; (a) 2.5 L initial stage of the reaction with substantial amounts of O-(2×1); (b) 7 L, almost all the O-(2×1) has been removed; 397×397 Å, 1 nA, 500 mV.

Annealing overlayers of the type shown in Fig. 12 to between 350 and 400 K resulted in formation of a mixed phase overlayer containing formate mostly in a (4×1) arrangement though also with some $c(2 \times 2)$, Fig. 14, to-

gether with patches of oxygen $c(6\times2)$. This transformation could also be observed with LEED, which additionally showed that further annealing above 430 K to decompose the formate left only the oxygen (2×1) pattern. Fig. 15 shows two STM pictures taken during exposure of a saturated oxygen (2×1) overlayer to formic acid at 350 K. (4×1) was again the predominant formate structure and was accompanied by formation of the $c(6\times2)$ oxygen structure. The $c(6\times2)$ was seen to form from an early stage of the reaction as shown in Fig. 15a while substantial areas of the surface were still covered with O-(2×1). The area of $c(6\times2)$ in Fig. 15b, which is taken in almost the same position on the surface, can clearly be seen to increase as the formate (4×1) grows to occupy the remainder of the surface. Haq and Leibsle [24] have previously reported small areas of (4×1) periodicity following adsorption of formic acid on oxygen precovered Cu(110) at 300 K, and they propose a structure consisting of alternate rows of formate and O–Cu–O chains parallel to the [001] direction. This structure would be consistent with the alternating light and dark close packed rows observed in the STM image of Fig. 14.

4.3. Reaction mechanism

From the complementary information presented above, a model of the reaction and oxidation of formic acid on Cu(110) can be proposed.

4.3.1. Formic acid on clean Cu(110)

This is characterised by a low reactive sticking coefficient at room temperature of about 0.1. The reaction here is:

$$HCOOH_{(g)} \rightarrow HCOOH_{(a)}, \quad (1)$$

$$HCOOH_{(a)} \rightarrow HCOO_{(a)} + H(a), \quad (2)$$

$$2H_{(a)} \rightarrow H_{2(g)}, \quad (3)$$

and step 2 may be slightly activated; this barrier may be reduced at the steps. The structure of the formate is discussed in detail in Ref. [20] and is composed of short formate rows offset in the $[1\bar{1}0]$ direction by one lattice spacing. The resultant coverage is a little below 0.25 ML (the local density within a domain) at saturation under these conditions. The mismatches between domains probably occur due to the competition between the long range repulsive interactions between molecules and the heat of adsorption of formic acid on the Cu(110).

4.3.2. Formic acid on low oxygen coverages

The reaction of formic acid with the added row O-(2×1) is energetically favourable and occurs readily at room temperature and above. The formic acid uptake is therefore, limited by the availability of reactive oxygen and not intermolecular repulsions, as on the clean surface, resulting in a higher total formic acid uptake. Additionally, the long, thin island structures formed (either (2×1) or (3×1)) create barriers to adatom diffusion. We believe that these barriers channel the Cu atoms liberated from the O-(2×1) islands by formate adsorption, so that these adatoms preferentially recombine with a step edge close to the barrier. This step then grows in a pyramid type fashion which is dictated by the diffusion of Cu atoms from the island edges into the step (Fig. 11).

4.3.3. Formic acid on high oxygen coverages

If we begin with 0.5 ML of oxygen, the formic acid can still react with high probability, but now the liberated Cu cannot diffuse over clean Cu, which it prefers to do, but diffuses slowly over the (2×1) oxygen layer instead. Furthermore, since two formate molecules are adsorbed per oxygen atom removed, the formate occupies more space on the surface than the removed O-(2×1) unit (the formate produces a (3×1) structure). This results in pressure on the oxygen layer and compression of the structure into a smaller space with higher oxygen coverage, forming the $c(6\times2)$ layer. This structure is relatively unreactive, as shown by the lower reaction probability of a complete overlayer of $c(6\times2)$ observed in the molecular

beam (< 0.02) and the higher doses needed to see this structure react using STM. Thus, at low doses, the reaction stops with a mix of $c(6 \times 2)$ oxygen and (3×1) formate on the surface, with about 0.5 ML of formate adsorbed, as shown by the beam data in Fig. 4. As the 0.5 ML of formate occupies only part of the surface it seems the most likely structure contains a local formate coverage of $2/3$ ML. The observation of two non-equivalent units in the unit cell with STM suggests a structure containing two rows of formate rows running parallel to the [001] direction, with the formate in the two rows adsorbed in different sites.

At high temperatures, no compression occurs because the formate is unstable, and the whole oxygen layer is removed, with the changed reaction stoichiometry of one oxygen atom removed per formic acid reacted. This leaves the surface clean.

At intermediate temperatures, where the molecular beam data show much reduced total uptake, the surface is dominated by a lower coverage formate structure—(4×1) rather than the (3×1) structure produced on room temperature formic acid adsorption. In Fig. 14, the (4×1) structure can clearly be seen to contain two components, probably alternating formate and O–Cu rows on the surface [24] and so producing a local formate coverage of 0.25 ML. Fig. 15 also shows formation of oxygen $c(6 \times 2)$ together with formate (4×1). Thus, much of the oxygen in the surface is trapped in the $c(6 \times 2)$ structure and is unavailable for reaction, a mechanism for oxygen passivation similar to that for adsorption at 300 K. In addition, the alternating formate and O–Cu rows which compose the (4×1) imply that once formic acid has removed a single O–Cu row, the neighbouring O–Cu rows become passivated and unreactive. Thus, the uptake rapidly drops as a small number of formate molecules adsorbing can deactivate a large number of oxygen atoms.

The lower local formate coverage in the (4×1) structure together with the accompanying oxygen deactivation explains the lower formic acid uptake at 350–400 K when compared with the uptake at 300 K which was observed with the beam data. The change in formate structure with sample temperature from (3×1) at low temperature to (4×1) at intermediate temperature is therefore important in understanding the surface reactivity.

The ability to combine STM and molecular beam measurements in this example allows us to construct detailed models of the surface dynamics and kinetics in what has proved to be a fascinating and complex system.

5. Conclusions

Here, we have illustrated the strength of combining a macroscopic, kinetic technique with a nanoscopic structural probe. This combination results in enhanced insight into the mechanisms of surface reactions, and especially into the importance of adsorbate structure and surface metal atom rearrangement and surface diffusion in those processes.

Acknowledgements

The authors are grateful to the following organisations for financial support: Oxford Instruments, the EPSRC, and the Universities of Liverpool and Reading.

References

[1] J.A. Dumesic, D.F. Rudd, L.M. Aparicio, J.E. Rekoske, A.A. Treviño, The Microkinetics of Heterogeneous Catalysis, American Chemical Society, Washington, DC, 1993.
[2] L. Kuipers, R.W.M. Loos, H. Neerings, J. ter Horst, G.J. Ruwiel, A.P. de Jongh, J.W.M. Frenken, Rev. Sci. Instr. 66 (1995) 4557.
[3] M. Bowker, P.D.A. Pudney, C.J. Barnes, J. Vac. Sci. Technol. A 8 (1990) 816.
[4] M. Bowker, Appl. Catal. A 160 (1997) 89.
[5] P. Mars, J.J.F. Scholten, P. Zwietering, Adv. Catal. 14 (1963) 35.

[6] K.C. Waugh, Catal. Today 15 (1992) 51.
[7] M. Bowker, Surf. Sci. Lett. 1 (1994) 542.
[8] M. Bowker, R.J. Madix, Surf. Sci. 102 (1981) 542.
[9] B.E. Hayden, K. Prince, D.P. Woodruff, A.M. Bradshaw, Surf. Sci. 133 (1983) 589.
[10] M. Bowker, S. Haq, R.P. Holroyd, P.M. Parlett, S. Poulston, N. Richardson, J. Chem. Soc., Faraday Trans. 92 (1996) 4683.
[11] A. Puschmann, J. Hasse, M.D. Crapper, C.E. Riley, D.P. Woodruff, Phys. Rev. Lett. 54 (1995) 2250.
[12] D.P. Woodruff, C.F. McConville, A.L.D. Kilcoyn, Th. Lindner, J. Somers, M. Surman, G. Paolucci, A.M. Bradshaw, Surf. Sci. 201 (1988) 228.
[13] J.L. Falconer, R.J. Madix, Surf. Sci. 46 (1974) 473.
[14] D.H.S. Ying, R.J. Madix, J. Catal. 61 (1980) 48.
[15] R.J. Madix, S.G. Telford, Surf. Sci. 277 (1992) 246.
[16] R.J. Madix, J.L. Gland, G.E. Mitchell, B.E. Sexton, Surf. Sci. 125 (1983) 481.
[17] N. Aas, Y. Li, M. Bowker, J. Phys.: Condens. Matter 3 (1991) 1.
[18] M. Bowker, E. Rowbotham, F.M. Leibsle, S. Haq, Surf. Sci. 349 (1996) 97.
[19] R. Feidenhansl, F. Grey, M. Nielsen, F. Besenbacher, F. Jensen, E. Laegsgaard, I. Stensgaard, K.W. Jacobsen, J.K. Nørskov, R.L. Johnson, Phys. Rev. Lett. 65 (1990) 2027.
[20] S. Poulston, R.A. Bennett, A.H. Jones, M. Bowker, Phys. Rev. B 55 (1997) .
[21] F.M. Leibsle, S. Haq, B.G. Frederick, M. Bowker, N.V. Richardson, Surf. Sci. 343 (1995) L1175.
[22] S. Poulston, A.H. Jones, R.A. Bennett, M. Bowker, Surf. Sci. 377-379 (1997) 66.
[23] P. Stone, S. Poulston, R.A. Bennett, M. Bowker, in preparation.
[24] S. Haq, F.M. Leibsle, Surf. Sci. 375 (1997) 81.